ACS APPLIED MATERIALS & INTERFACES

Research Article

www.acsami.org

Li Storage and Impedance Spectroscopy Studies on Co_3O_4, CoO, and CoN for Li-Ion Batteries

M. V. Reddy,*[†,§,⊥] Gundlapalli Prithvi,[†,‡] Kian Ping Loh,[§] and B. V. R. Chowdari[‡]

[†]Department of Physics, Solid State Ionics & Advanced Batteries Lab, [§]Department of Chemistry, Graphene Research Center, and [⊥]Departments of Materials Science & Engineering, National University of Singapore, Singapore 117542

[‡]St Andrew's Junior College, 5 Sorby Adams Drive, Singapore 357691

Supporting Information

ABSTRACT: The compounds, CoN, CoO, and Co_3O_4 were prepared in the form of nano-rod/particles and we investigated the Li-cycling properties, and their use as an anode material. The urea combustion method, nitridation, and carbothermal reduction methods were adopted to prepare Co_3O_4, CoN, and CoO, respectively. X-ray diffraction (XRD), scanning electron microscope (SEM), transmission electron microscope (TEM), and the Brunauer–Emmett–Teller (BET) surface and density methods were used to characterise the materials. Cyclic voltammetry (CV) was performed and galvanostatic cycling tests were also conducted up to 60–70 cycles. The observed reversible capacity of all compounds is of the increasing order CoO, Co_3O_4, CoN and all compounds showed negligible capacity fading. CoO allows for Li_2O and Co metal to form during the discharge cycle, allowing for a high theoretical capacity of 715 mA h g^{-1}. Co_3O_4 allows for 4 Li_2O and 3Co to form, and has a theoretical capacity of 890 $mAhg^{-1}$. CoN is the best anode material of the three because the nitrogen allows for Li_3N and Co to form, resulting in an even higher theoretical capacity of 1100 $mAhg^{-1}$ due to the Li_3N and Co metal formation. Irrespective of morphology the charge profiles of all three compounds showed a major plateaux ~2.0 V vs. Li and potential values are almost unchanged irrespective of crystal structure. Electrochemical impedance spectroscopy (EIS) was performed to understand variation resistance and capacitance values.

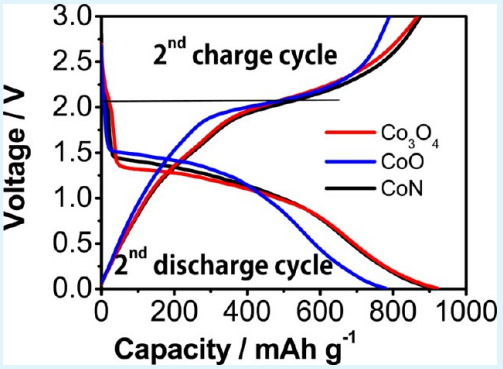

KEYWORDS: *CoN, CoO, Co_3O_4, lithium-ion batteries, anode materials, bulk preparation methods, electrochemical characteristics*

INTRODUCTION

Lithium-ion batteries have become increasingly popular in today's world as portable gadgets see a rise in popularity. These batteries have a fairly high capacity, are rechargeable, and have a good design and are easy to manufacture. This has made them a good choice for powering electronics.[1] Batteries are being used in many devices today such as phones, laptops, and more recently in hybrid cars like the Toyota Prius and all-electric cars such as the Nissan Leaf and Tesla Roadster. However, conventional Li-ion batteries are not ideal choices for high power applications. Firstly, they use $LiCoO_2$ as the cathode[2] and graphite as the anode and this combination results in the formation of potentially dangerous dendrites when cycling at high current rates.[3] The graphite anode also has a low theoretical capacity of 372 mA h g^{-1}. As an increasing number of devices today require more power and as batteries start seeing use in vehicles, it is necessary to explore other anode materials that can offer greater capacity while still remaining economically viable.

The anodic properties of Co_3O_4 and CoO were first reported by Poizot et al. in year 2000[4] and CoN thin films were reported by Das et al.[5] Other recent studies of various metal oxides have been adequately reviewed by Cabana et al[6] and Reddy et al.[7] Some of the recent additional reports on nanostructured materials were reported in the form of interconnected network type particles,[8] nano/submicrometer sized particles,[9] nanowires,[10,11] nanowires arrays,[12,13] nanofibers,[14−17] nanotubes,[18] nanowalls,[19] nanosheets,[20] microbelts,[21] microspheres,[22] etc.

In literature, Co_3O_4 has been extensively investigated as an anode material, because this material can be easy to prepare in comparison to CoO or Co_2O_3. It can be easily prepared by Co-containing different salts like nitrates, acetates, hydroxides, carbonates, oxalate, and sulphates upon heating in air above 200–400°C in air by various conventional methods such as the solid state method, hydrothermal method,[23] precipitation,[24] virus-enabled synthesis,[25] template method,[26] ammonia-evaporation-induced method,[12,13] molten salt method,[27,28] thermal decomposition,[29] physical methods,[30] etc.,[7] and the various morphologies have been well summarized in recent reviews.[6,7] To summarise the anodic properties of Co_3O_4; many reports reproduced the reported capacity values and conversion mechanism proposed by Poizot et al.[4] Many published reports showed an initial reversible capacity larger than the theoretical capacity of Co_3O_4, and higher reversible capacities were

Received: October 29, 2013
Accepted: December 10, 2013
Published: December 10, 2013

reported depending on preparation method and fabrication technique. Among all, nanowire arrays had a reported reversible capacity of 450 and 240 mA h g^{-1} at 20*C* and 50*C* rate, respectively,[12] and similar capacity values were reported on virus-based synthesis methods.[25]

The CoO has a cubic rock salt type structure, conversion and displacement reaction of CoO by Poizot et al.[4] showed a reversible capacity of 700 mA h $g^{-1.}$ Discharge−charge reaction mechanism, formation mechanism of Solid Electrolyte interface (SEI), polymeric layer formation of CoO by various techniques such as XRD, TEM and XPS techniques extensively studied by group of Tarascon are summarized in the recent review report.[7] Latter CoO prepared in the form of micrometer/Nano sized particles,[4] nano discs,[31] Nanocages,[32] nano platelets and composites of Carbon/graphene[33] and other nano composites[34,35] are given in recent report.[7] The observed reported reversible capacities are within the range of 640−1080 mA h g^{-1}.

Li-cycling properties of CoN thin film,[5] bulk CoN,[36] Ni-doped CoN,[37] and other nitrides are summarized by Cabana et al.[6] Other Nitrogen containing materials have been studied for pseudo capacitor applications.[38−42] Previously Das et al.[36] reported preparation of bulk CoN at 335 °C. Finding the right temperature was important because heating the Co_3O_4 sample in presence of ammonia to higher temperature (those above 400 °C) leads to the formation of other phases like Co_2N and Co metal, which affect the purity of the final compound. Presently, we used a slightly lower preparation temperature (300 °C) when compared to previous report (350 °C). To the best of our knowledge, there are not many reports on the fundamental aspects of these materials or on the comparative studies of the above materials

The aim of this project is to understand the effect of the crystal structures and preparation temperature of Co_3O_4, CoN and CoO charge and discharge voltage profiles and its evaluation of capacity values. Carbothermal reduction, nitridiation and urea combustion methods were used to prepare CoO, CoN and Co_3O_4 respectively. We used these bulk preparation methods to produce the above mentioned materials in gram quantities and report the comparative Li-cycling studies of the three materials. Electrochemical studies of the materials were also performed to assess the effectiveness of the bulk preparation methods. XRD was performed to analyse purity and structure of the compounds. BET surface and density methods and SEM were used to characterise the materials. Cyclic voltammetry, galvanostatic cycling and impedance spectroscopy were used to analyse the electrochemical properties and reaction kinetics of the materials.

EXPERIMENTAL SECTION

Preparation of Materials. *Preparation of Co_3O_4.* Co_3O_4 was prepared by dissolving $Co(CH_3COO)_2{\cdot}xH_2O$ (Alfa Aesar; 98%) and urea in distilled H_2O in a glass beaker using a magnetic stirrer. Urea act as an oxidising fuel. The metal salt to urea mole ratio is 1:4. The mixture was slowly evaporated to dryness on a hot plate, followed by heating at 280 °C for 6 h in air in a box furnace (Carbolite, U. K.). The Co_3O_4 powder was also used as a precursor for the preparation of CoO and CoN materials.

Preparation of CoO. Initially we attempted to synthesize CoO from Co_3O_4 by urea combustion method and also by heating in Argon gas at 600°C for 6 h. However, this method was unsuccessful. Hence we adopted a carbothermal reduction using Co_3O_4 as a precursor. By using the carbothermal method, we have prepared a variety of metal cluster compounds[43,44] and $LiVPO_4F$.[45] The carbothermal reduction method is a simple method to reduce the metal oxides to a lower oxidation state using carbon as a reducing agent.

One and a half grams of Co_3O_4 was used, corresponding to 0.07478 g of carbon (using stoichiometric ratios). An additional 20% of carbon was added to ensure the reaction went to completion. Hence, a total of 0.08974 g of carbon was used. The Co_3O_4 was placed on a clean alumina boat and was first heated to 600°C for 6 h in a tubular furnace (Carbolite, UK) in an argon atmosphere, again re-heated at 700°C for 6 h in argon atmosphere to obtain a pure CoO phase. The following reaction mechanism was proposed for the carbothermal reduction:

$$Co_3O_4(s) + C(s) \rightarrow 3CoO(s) + CO(g)$$

Preparation of CoN. Co_3O_4 was used as a precursor to synthesize CoN via a nitridation method. The precursor was placed in the tubular furnace and heated with Ammonia/N_2 gas for 4h at 300°C. We used a lower preparation temperature for CoN as compared to a previous report on bulk CoN prepared at 335°C.[36] We note that the initial porosity of the Co_3O_4 sample plays an important role on the penetration of ammonia/N_2 gas, and we also attempted to prepare CoN using a different source of Co_3O_4, i.e., dense Co_3O_4 prepared using the molten salt method[28] and results showed the presence of unreacted Co_3O_4 in addition to CoN.

Electrode Fabrication. The anodes were manufactured using the above compounds as the active material, polyvinylidene fluoride (PVDF) as a binder, and Super-P carbon as a conductive additive in the weight ratio of 70:15:15. *N*-Methyl-2-pyrrolidone (NMP) was used as a solvent. Super-P carbon and the anode material were ground in a mortar and pestle to very fine powders. PVDF binder was added in the mass ratio stated above. NMP was then added till the slurry was of an appropriate viscosity. A magnetic stirrer was placed in the vial and the vial was placed on a magnetic stirring plate overnight to ensure a uniform slurry was obtained. The slurry was then used to coat a copper foil substrate to a thickness of 25 μm using the doctor blade technique.[46] The foil was placed in an oven at 80 °C overnight and then roller-pressed to increase contact between foil and anode material. Discs of diameter 1.6 cm (2.0 cm^2 geometric area) were cut using an electrode cutter. The mass of the active material used in making the Co_3O_4, CoO, and CoN anodes are 3.43 mg, 5.25 mg, 2.87 mg respectively. The electrodes were then placed in a vacuum oven overnight to completely dry. Coin cells (CR2016) were used in the cell fabrication. Lithium metal was used as the cathode and 1M Lithium hexafluorophosphate ($LiPF_6$) (0.5M EC:0.5M DEC) (Merck) was used as the electrolyte.

Characterization Techniques. The X-ray diffraction (XRD) patterns were taken using Cu Kα radiation (Advance D8, Bruker). Rietveld refinement was performed on all three compounds using the TOPAS software (version 2.1). Scanning electron microscopy (SEM) (JEOL, JSM 67500F) and Transmission electron Microscope (TEM) (JEOL JEM 2010, operating at 200 kV)) images of all three compounds were taken to determine the surface morphology and the particle sizes. The BET surface method (Micromeritics TriStar, USA) was used to investigate the surface area of the compounds. The Bitrode multi-channel tester (MCV16-05/001-5, Bitrode, USA) was used for galvanostatic charge−discharge cycling of the batteries. It gives information of capacity values and capacity fading. CV was performed using a multi-potentiostat (Macpile II, Biologic, France). Electrochemical impedance spectroscopy (EIS) was performed on the Solartron Impedance/gain-phase analyzer (SI 1255) with a potentiostat (SI 1268) at room temperature. More details on the electroanalytical techniques have been reported previously.[47,48]

RESULTS AND DISCUSSION

Structure and Morphology. The Rietveld refined X-ray patterns of all compounds are shown in Figure 1. The compounds showed a lattice parameter values of "*a*" = 8.0876(3), 4.2608(5), 4.2485(5) Å, respectively for Co_3O_4, CoO, and CoN, respectively. They were refined using the known reported space group Fm-3m (225) for CoO, cubic

dx.doi.org/10.1021/am4047552 | ACS Appl. Mater. Interfaces 2014, 6, 680−690

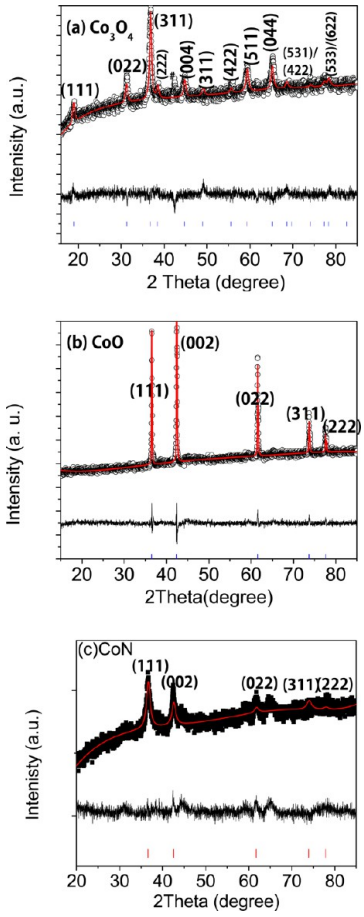

Figure 1. Rietveld refined XRD patterns of (a) Co_3O_4, (b) CoO, and (c) CoN. Vertical lines are (*hkl*) lines of CoO, CoN, and Co_3O_4 and difference patterns are shown. Recorded with CuKα radiation. A minor unknown peak is also seen in a and c.

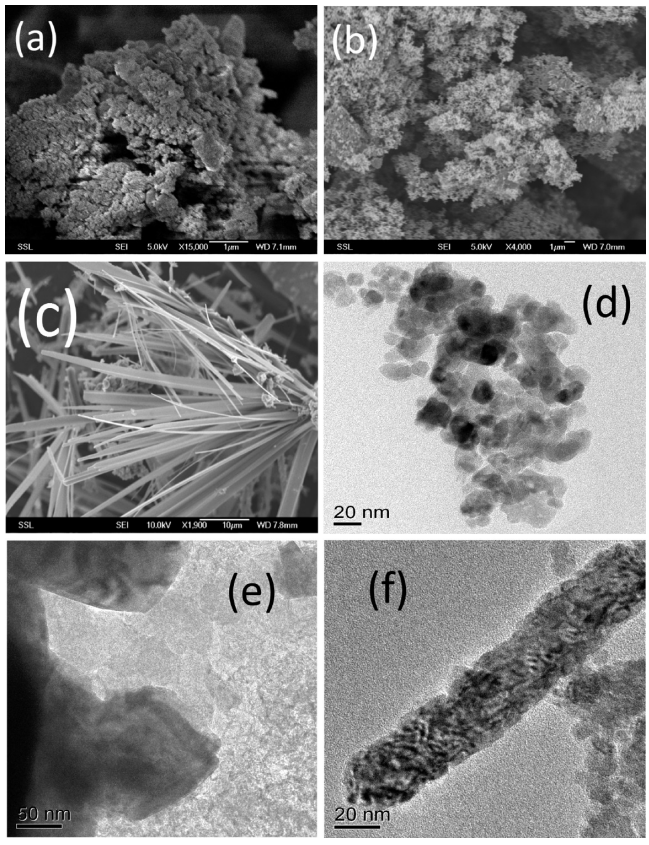

Figure 2. Scanning electron microscopy (SEM) images of compounds: (a) Co_3O_4, 15k magnification, scale bar 1 μm, (b) CoO, 4k magnification, scale bar 1 μm, (c) CoN, 1.9K magnification, scale bar 10 μm; and transmission electron microscopy (TEM) images of (d) Co_3O_4, scale bar 20 nm, (e) CoO, scale bar 50 nm, and (f) CoN, scale bar 20 nm.

FCC structure space group F-43m (216) for CoN and Fd-3m (227) for Co_3O_4. The average crystallite size of Co_3O_4, CoO, and CoN, (calculated using TOPAS software) are: 16, 118, and 8.9 nm, respectively. We noted that the average crystallite size of CoN decreases from 19 to 8.9 nm with the preparation temperature from 335[36] to 300 °C. Our observed lattice parameter value of Co_3O_4 are close to previous reports on Co_3O_4 prepared by precipitation method at 250°C by Godillot et al.[49] and also molten salt method by Reddy et. al.[27] and lattice parameter values of CoN are close to previous reports[5,36] and a slight differences in the lattice parameter was noted with Ni-doped CoN.[37] We note a minor phase of unreacted unknown peaks are also seen in panels a and c in Figure 1; further careful studies using Neutron diffraction, Synchrotron X-ray diffraction and high-resolution XRD patterns using Co−Kα radiation are needed.

SEM and TEM images of Co_3O_4, CoO, and CoN compounds are shown in Figure 2. Co_3O_4 showed submicrometer sized agglomerated particles is order of 10−20 nm (Figure 2a, d). CoO showed a coral-like structure (Fig.2b) and submicrometer sized CoO particles was noted from TEM studies (Figure 2e). CoN has a micro/nanorod/belt-type morphology (Figure 2c, f) and in addition to rod type morphology, a agglomerates of nanoparticles are also seen from TEM image (Figure 2f). All the prepared powders are black in colour and BET surface area of powders of Co_3O_4, CoO and CoN are 29, 11.8, and 27.6 (± 0.2 $m^2\ g^{-1}$), respectively. The decrease in BET surface area of CoO was correlated to the higher synthesis temperature used in this project. A similar decrease of BET surface area was noted with other metal cluster compounds such as MMo_3O_8 (M = LiY, LiHo, Mn_2)[43,44] using the carbothermal reduction method and this was mainly attributed to the high temperature reaction. In addition to the above, surface area is known to vary depending on the method of preparation and morphology. For example, Co_3O_4 compounds prepared using the molten salt method have surface areas in the range of 0.77 to 19 $m^2\ g^{-1}$[27,28] and CoO nano disks reported by Sun et al.[31] showed a surface area of 33 $m^2\ g^{-1}$. Higher BET surface areas may be associated with higher reversible capacities as more lithium is able to react with the anode material at higher current rates and also greater electrolyte permeability with the active material.[7]

Electrochemical Characteristics. *Galvanostatic Cycling Studies of Co_3O_4, CoO, and CoN:* Galvanostatic charge−discharge cycling is used to study capacity value variations, understand discharge−charge profiles and coulombic efficiency of the cell. The voltage range used was 0.005−3.0 V vs. Li and carried out a current rate of 60 mA g^{-1}.

Co_3O_4. Galvanostatic cycling graphs of 1st, 2nd, 40th, and 50th charge and discharge cycles with the voltage vs. capacity as well as capacity and capacity vs. cycle number plots are shown in Figure 3a, b. These are important cycles that show the structural destruction during charge and discharge cycles.

dx.doi.org/10.1021/am4047552 | ACS Appl. Mater. Interfaces 2014, 6, 680−690

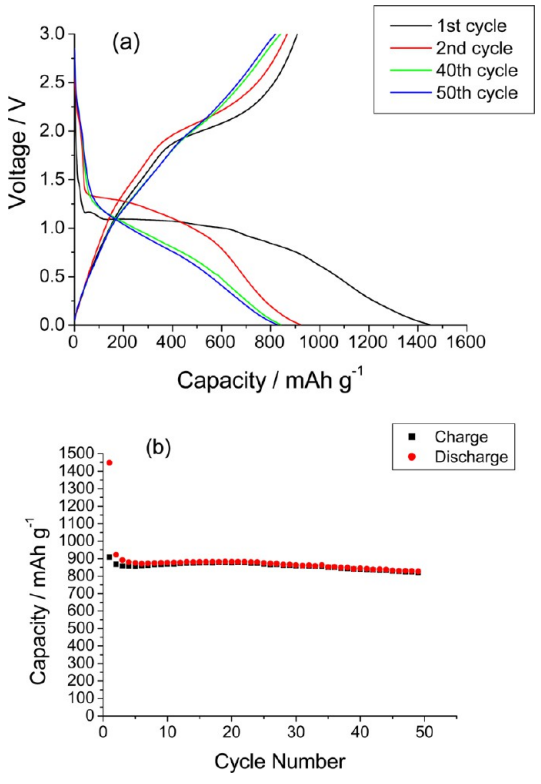

Figure 3. Co_3O_4 (a) voltage vs. capacity graphs of certain cycles, (b) capacity vs. cycle number plots at current rate 60 mA g^{-1}, voltage range, 0.005−3.0 V vs. Li.

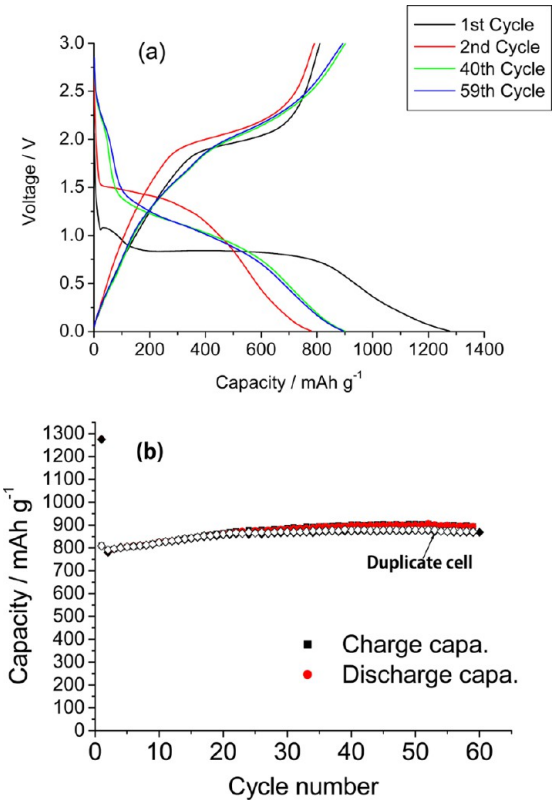

Figure 4. CoO (a) voltage against capacity of certain cycles (b) capacity vs. cycle number over 60 cycles. Voltage range, 0.005−3.0 V vs. Li, current rate, 60 mA g^{-1}. Duplicate cell cycled up to 60 cycles are also shown.

During the first discharge cycle, the voltage drops sharply from the open-circuit voltage (OCV) of about 2.8 V to about 1.2 V. This corresponds to the beginning of the insertion of Li^+ ions into the Co_3O_4 structure. The corresponding capacity observed is about 115 mAh g^{-1}. The discharge profile mainly consists of a voltage plateau at about 1.1 V. At about 1.0 V, the voltage starts dropping with a gentle sloping profile. This sloping portion covers a capacity of about 950 mAh g^{-1}. The overall capacity at the end of the first deep discharge is 1450 (±5) mAh g^{-1}. The first charge cycle has no voltage plateau, but has a sloping profile that changes at about 1.8 V till about 2.2 V. This accounts for a capacity of about 290 mAh g^{-1}. During charge cycle, the Co_3O_4 or CoO/Co_3O_4 reforms. At the end of the first charge cycle the capacity is 908 mAh g^{-1}. There is an irreversible capacity loss (ICL) of 541 mAh g^{-1}. Similar ICL is commonly observed in many other metal oxides and reports on Co_3O_4.[6,7,27,50−52] The first-cycle ICL is due to the formation of the solid electrolyte interface (SEI), formation of gel-type polymeric layer and also partially due to the reduction of the solvent in the electrolyte.[6,7,27,30,36,37,50]

The second discharge cycle has a very different profile, indicating a different electrochemical reaction. The voltage plateau originally seen at 1.1 V is no longer seen. Instead, the sloping profile changes at 1.4 V. This sloping profile varies until 0.005 V. The capacity at the end of the second discharge cycle is 922 mAh g^{-1}. The second charge cycle is analogous to the first charge cycle, which indicates that similar electrochemical reactions are taking place in both these cycles. A high capacity of 867 mAh g^{-1} was observed at the end of the second charge cycle. The discharge cycles from 2-40 cycles differs again. The voltage plateau is at about 1.2 V at the 40th cycle. The capacity at this voltage is about 100 mAh g^{-1}. The voltage decreases linearly till the end of the discharge cycle at 0.005 V. The capacity at the end of the 40th discharge cycle is 842 mAh g^{-1}. The charge cycle also differs. There is no longer any voltage plateau and the voltage increases linearly with capacity. The capacity at the end of the 40th charge cycle is 840 mAh g^{-1}. The 40−50 cycles are analogous in their behaviour in the cycling profiles. The 50th discharge cycle capacity is 827 mAh g^{-1} and the charge cycle capacity was 819 mAh g^{-1}. The cell displayed excellent capacity retention and columbic efficiency over 50 cycles with a good capacity retention was 94.5% (Table

Table 1. Reversible Capacity and Capacity Retention Values of Co_3O_4 and CoO and CoN

compound	1st cycle reversible capacity (mA h g^{-1})	2nd cycle reversible capacity (±5 mA h g^{-1})	reversible capacity (±5 mA h g^{-1}) at *n*th cycle	capacity retention
Co_3O_4 (60 mA g^{-1})	908	867	819 (50 cycles)	94.5%
Co_3O_4 (120 mA g^{-1})	881	802	620 (67 cycles)	77.3%
CoO; 60 mA g^{-1}	811	790	893 (60 cycles)	nill (capacity increase with cycle number)
CoN 60 mA g^{-1}	919	875	956 (60 cycles)	nill (capacity increase)

dx.doi.org/10.1021/am4047552 | ACS Appl. Mater. Interfaces 2014, 6, 680−690

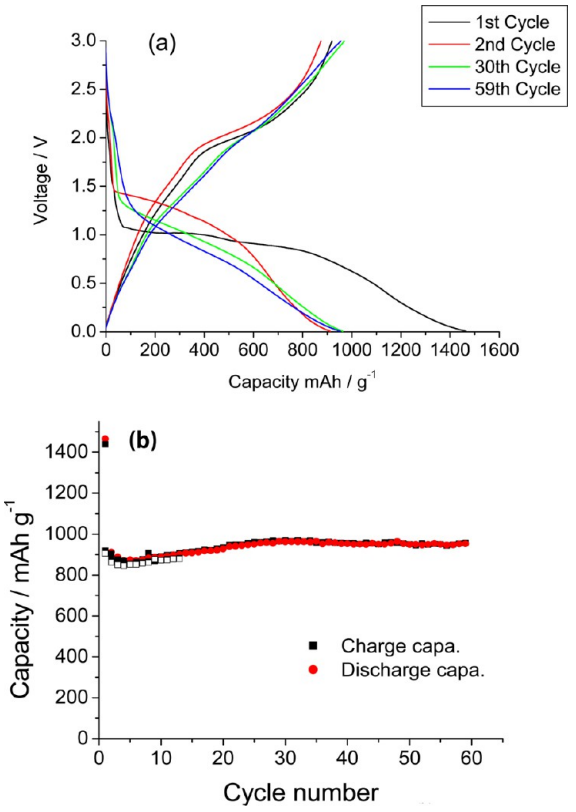

Figure 5. CoN (a) voltage against capacity of certain cycles, (b) capacity vs. cycle number over 60 cycles; voltage range, 0.005−3.0 V vs. Li, current rate, 60 mA g^{-1}. Duplicate cell cycled up to 14 cycles are also shown.

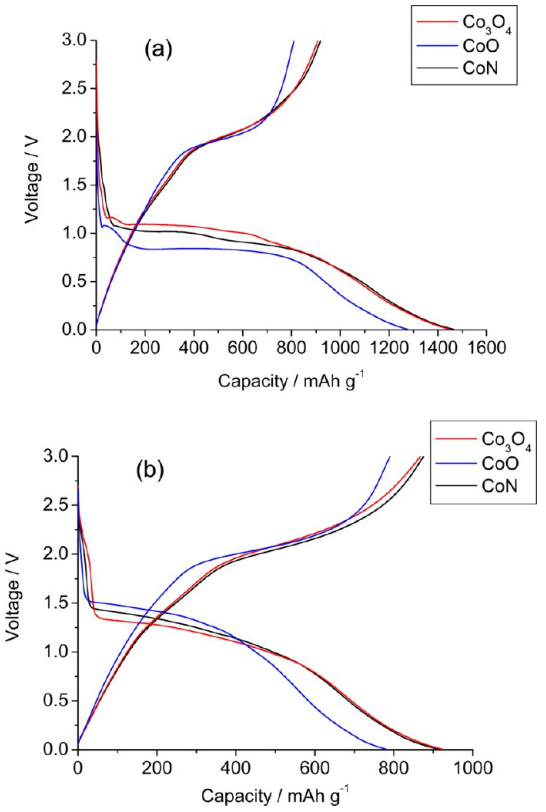

Figure 6. Comparative first and second cycle charge-discharge plots of voltage vs. capacity of CoO, Co_3O_4 and CoN: (a) first cycle and (b) second cycle. Voltage range, 0.005−3.0 V vs. Li, current rate, 60 mA g^{-1}.

1). The proposed reaction mechanisms during charge and discharge cycles are based on previous studies[6,7,28,50]

$$Co_3O_4 + xLi^+ + xe^- \rightarrow Li_xCo_3O_4 + (8-x)Li^+ + (8-x)e^- \rightarrow 3Co + 4Li_2O \text{ (discharge)} \quad (1)$$

$$3Co + 3Li_2O \rightleftharpoons 3CoO + 6Li^+ + 6e^- \text{ (charge)} \quad (2)$$

$$3Co + 4Li_2O \rightleftharpoons Co_3O_4 + 8Li^+ + 8e^- \text{ (charge)} \quad (3)$$

The purpose of using a higher current rate was to determine whether a similar capacity and columbic efficiency could be achieved as compared to the cell at the lower current rate. Generally, a higher current rate results in poorer performance due to differences in the Li-ion kinetics. The cell was put through 67 charge-discharge cycle profiles at a current rate of 120 mA g^{-1} are shown in Figure S1 in the Supporting Information and the proposed reaction mechanism was the same as the cell at lower current rate. During the discharge cycle, the voltage drops sharply from the OCV of about 2.3 V to about 1.2 V. This shows the insertion of lithium ions into the crystal structure. The corresponding capacity at this voltage is only about 40 mAh g^{-1}. There is a small voltage plateau at about 1.1 V, followed by a sloping profile till just above 0.005 V. This slope account for about 925 mAh g^{-1} of the capacity. The discharge cycle continues with a new plateau till 0.005 V. This plateau accounts for about 375 mA h g^{-1} of the capacity. The first cycle deep discharge capacity is 1347 mA h g^{-1}. The charge cycle has no plateau. It has a sloping profile that changes at about 1.9 V till about 2.3 V, before changing again. The capacity at the end of the first charge cycle was 881 mAh g^{-1}. This first cycle of this cell is similar to the first cycle of the cell at lower current rate, apart from the plateau at the end of the first discharge cycle. Without this plateau, the first cycle discharge capacity would be similar to that of the cell at a lower current rate. The voltage drops sharply from 3.0 to 1.4 V, and then slopes downward till 0.005 V with no plateau. The capacity at the end of the second discharge cycle is 842 mAh g^{-1}. The second charge profile is analogous to the first charge profile, indicating similar electrochemical reactions. The capacity at the end of the second charge cycle is 802 mAh g^{-1}. The whole second cycle is very similar to the whole second cycle of the cell at lower current rate. The difference is the capacity at the end of the cycle. As expected the observed capacity is lower at the higher current rate due kinetics limitations. The 30th discharge cycle capacity is 740 mAh g^{-1}. However, the 2−30 charge cycles are different. The charge cycle is linear without any significant change in the gradient. The capacity at the end of the 30th charge cycle is 734 mAh g^{-1}. The 30−67 charge and discharge cycles are analogous. The capacity at the end of the 67th discharge cycle is 628 mAh g^{-1}. The capacity at the end of the 67th charge cycle is 620 mAh g^{-1}.The cell showed good coulombic efficiency and capacity retention. The capacity retention over 67 cycles was 77.3%. Predictably, this is lower than the cell at lower current rate of 60 mA g^{-1} for reasons explained above. We note that depending on method of preparation, morphology variation and other factors like weight of the active material, geometrical area of the electrode and fabrication techniques a differences in the

dx.doi.org/10.1021/am4047552 | ACS Appl. Mater. Interfaces 2014, 6, 680−690

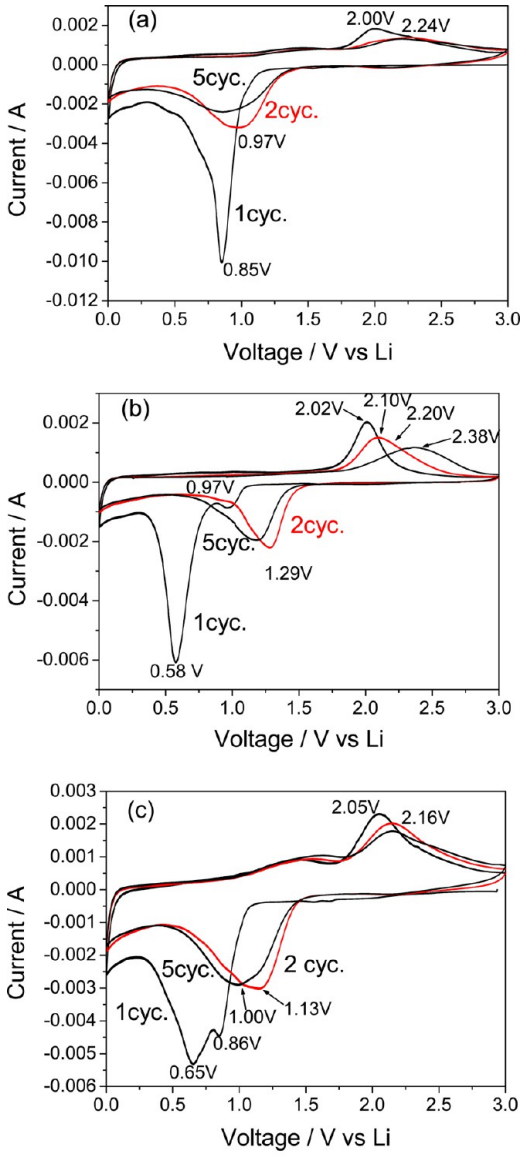

Figure 7. Cyclic voltammograms of (a) Co_3O_4, (b) CoO, and (c) CoN, voltage range, 0.005–3.0 V vs. Li, scan rate 58 $\mu V\ s^{-1}$.

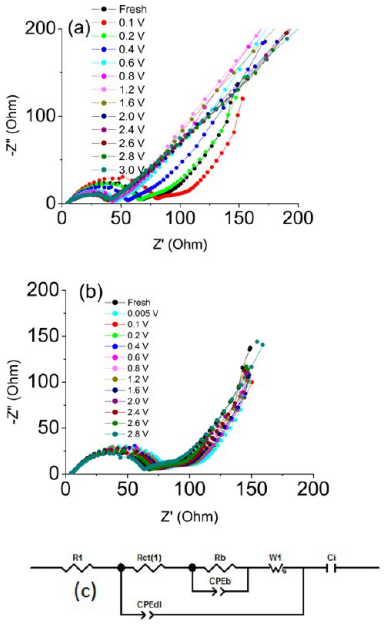

Figure 8. Nyquist plots ($-Z''$ vs. Z') of Co_3O_4 (a) charge cycle , (b) discharge cycle, and (c) equivalent electrical circuit.

capacity values were reported by various groups are nicely summarized in the review by Reddy et al.[7] and other recent studies on Co_3O_4 nanostructures are.[53−63]

CoO. The discharge−charge cycling curves and capacity vs. cycle number plots of CoO are shown in Fig.4a,b. During the first discharge cycle, the voltage dropped suddenly from the OCV of 2.1 V to 1.05 V, before rising slightly to 1.1 V. This is the beginning of the insertion of lithium ions into the CoO crystal structure. Capacity at this voltage is just 24 mAh g^{-1}. The voltage then plateaus at about 0.85 V, corresponding to a capacity of about 170 mAh g^{-1}. This large plateau continues till the capacity reaches about 800 mAh g^{-1}. The voltage then follows a sloping profile till the cut-off at 0.005 V. The overall capacity at the end of the first discharge cycle is 1276 mAh g^{-1}. The first charge cycle has a sloping profile that changes at 1.8 V till 2.1 V. This accounts for about 315 mAh g^{-1} of the capacity. The capacity at the end of the first charge cycle is 811 mAh g^{-1}. There is an ICL of 466 mAh g^{-1} and reasons for ICL are similar to Co_3O_4. The proposed reaction mechanism is as follows[4,7]

$$CoO + 2Li + 2e^- \rightleftharpoons Co + Li_2O \text{ (discharge)} \quad (4)$$

$$Co + Li_2O \rightleftharpoons CoO + 2Li^+ + 2e^- \text{ (charge)} \quad (5)$$

The second cycle discharge is different from the first cycle discharge, indicating a different electrochemical reaction. There is not voltage plateau in this cycle. Instead, the voltage drops sharply to about 1.5 V, where the capacity is about 25 mAh g^{-1}, and then decreases linearly till about 1.35 V, where the capacity is about 265 mAh g^{-1}. The voltage then drops in a smooth curve till the cut-off at 0.005 V. The total capacity at the end of the second discharge cycle is 780 mAh g^{-1}. The second charge cycle is analogous to the first charge cycle, indicating similar electrochemical reactions. The capacity at the end of the second charge cycle is 790 mAh g^{-1}. The voltage drop is not as sharp as before and the sloping profile now changes at about 1.4 V. The capacity at this voltage is about 105 mAh g^{-1}. The voltage then decreases fairly linearly till 0.005 V. The capacity at the end of the 40th discharge cycle is 899 mAh g^{-1}. The gradient for the 40th charge cycle is fairly constant throughout, and the capacity at the end of the 40th charge cycle is 902 mAh g^{-1}. The 40-60 charge and discharge cycles are analogous and almost overlapping, indicating very similar electrochemical reactions and capacity between these cycles. The 60th discharge cycle capacity is 895 mAh g^{-1} and the charge cycle capacity is 893 mAh g^{-1} (Table 1) (Figure 4b) .

The cell has excellent columbic efficiency and interestingly, the cell did not undergo capacity fading. Instead, capacity at the 59th cycle was 13.0% higher than the capacity at the 2nd cycle (Fig.4b). Further studies need to be conducted to analyse the reasons for this. It is also interesting to note that the actual capacity of the CoO cell has far exceeded the theoretical capacity of 715 mAh g^{-1}. Even when comparing the last charge cycle capacity with the theoretical capacity, CoO exceeded the theoretical capacity by 25%. We note duplicate cell is also showed a similar capacity values are within the experimental error. Though a few papers have reported such higher-than-theoretical capacity (max. value of 1100 mAh/g),[31,64,65] the exact mechanism is not clear. One possible reasons for

dx.doi.org/10.1021/am4047552 | ACS Appl. Mater. Interfaces 2014, 6, 680−690

Table 2. Fitted Impedance Values of Co_3O_4 during Discharge and Charge Cycle at Selected Voltages

	R_1 (Ohm)	R_{ct} (Ohm)	R_b (Ohm)	CPE_b (F)	CPE_{dl} (F)
potential (charge)					
fresh cell	5.664	62.88	19.55	0.036017	4.9957×10^{-5}
0.4 V	5.716	50.83	13.46	0.07081	6.2507×10^{-5}
0.8 V	5.656	37.92	9.57	0.081415	9.0268×10^{-5}
1.6 V	5.123	35.22	6.55	0.037303	0.0001679
2.0 V	5.001	36.1	10.3	0.053752	0.00018061
2.4 V	4.732	36.53	9.65	0.065434	0.00019388
2.8 V	4.406	39.1	12.43	0.057337	0.00018574
3.0 V	4.39	39.25	4.32	0.22919	0.00016929
potential (discharge)					
fresh cell	5.664	62.86	20.47	0.03591	4.9856×10^{-5}
0.005 V	5.666	77.22	23.39	0.026637	4.5856×10^{-5}
0.1 V	5.694	75.51	25.59	0.026921	4.3401×10^{-5}
0.4 V	5.653	74.48	23.15	0.026982	4.5381×10^{-5}
0.8 V	5.569	72.14	24.83	0.028193	4.7677×10^{-5}
1.6 V	5.557	71.31	20.78	0.026768	4.7988×10^{-5}
2.0 V	5.501	68.66	22.31	0.028029	4.965×10^{-5}
2.4 V	5.472	68.18	22.03	0.027409	5.0262×10^{-5}
2.8 V	5.406	58.98	24.53	0.031073	5.6573×10^{-5}

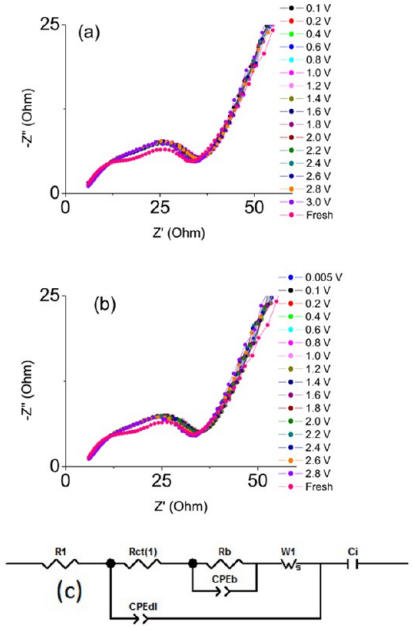

Figure 9. Nyquist plots ($-Z''$ vs. Z') of CoO (a) charge cycle, (b) discharge cycle, and (c) equivalent electrical circuit.

increases of capacity with initial cycles are due to formation cycle is that during the cycling process, a good contact is achieved between active material, binder, carbon, and current collectors, causing more active material participates during the electrochemical cycling. The electrocatalytic effect and the electrolyte also influence the increase in capacity. This effect occurs in other electrode materials.[7,44,45,66,67] Our reported capacity values are close to previous reports on CoO/Graphene composites,[33] slightly higher than the CoO nano cages (807 mAh g^{-1} at 0.2*C* rate)[32] and the other reports are summarized in our recent review.[7]

CoN. The electrochemical cycling profiles and capacity vs. cycle number plots are shown in Fig. 5. The voltage dropped from the OCV of 2.65 V to about 1.1 V. Capacity at this voltage was about 65 mAh g^{-1}. There was a small voltage plateau till the capacity reached about 460 mAh g^{-1}, the voltage then dropped with a sloping profile till the cut-off at 0.005 V and it showed a first discharge cycle capacity of 1465 mAh g^{-1}. The first charge cycle had a sloping profile that changed at about 1.8 V. The corresponding capacity was 380 mAh g^{-1}. The voltage continued increasing with an increasing gradient till 3.0 V. The first cycle charge capacity was 919 mAh g^{-1}. There is an ICL of 546 mAh g^{-1}, due to SEI formation and also partially due to reduction of the solvent are similar to other Co-oxides.

The second discharge cycle had a different profile. The voltage dropped initially to about 1.45 V. The capacity was about 35 mAh g^{-1}. The voltage then decreased steeply to 0.005 V and the final second discharge cycle capacity was 912 mAh g^{-1}. The second charge cycle was analogous to the first charge cycle, indicating similar electrochemical reactions. The second charge cycle capacity was 875 mAh g^{-1} and 30th discharge cycle has more gradual curves and the voltage drops is now till about 1.35 V. The voltage decrease is fairly linear from this voltage till the cut-off at 0.005 V. The 30th discharge cycle capacity is 963 mAh g^{-1}. The 30th charge cycle is similar to the second charge cycle, except that it is more linear and it showed a charge cycle capacity of 970 mAh g^{-1}. The 30th–59th charge and discharge cycles are analogous. The 59th discharge cycle capacity is 953 mAh g^{-1} and the 59th charge cycle capacity is 956 mAh g^{-1} (Table1). The proposed reaction mechanism for charge and discharge cycles based on the above studies is as follows:[5,36] $CoN + 3Li + 3e^- \rightleftharpoons Co + Li_3N$ ie during discharge is forward reaction, charge cycle is the reverse reaction. Observed bulk CoN capacity values are lower when compared to electrochemical performance of CoN thin films.[5] Also we note minor extra peak voltages were noted in discharge–charge profiles of thin film CoN, which is probably due to difference in the morphology[5] and good contact between the active material and current collector.[68] Another possible reason is that generally well resolved peaks are obtained with thin film electrodes.[69]

The reversible capacity and retention values with cycle number are listed in Table 1. Over 60 cycles, the capacity increase was 9.3% and capacity had increased from the 2nd cycle to the 35th cycle and the explanation for increase of capacity with cycle is similar to the case of CoO. From the 35th

dx.doi.org/10.1021/am4047552 | ACS Appl. Mater. Interfaces 2014, 6, 680–690

Table 3. Fitted Impedance Values of CoO during Discharge and Charge Cycle at Selected Voltages

	R_1 (Ohm)	R_{ct} (Ohm)	R_b (Ohm)	CPE_b (F)	CPE_{dl} (F)
potential (charge)					
fresh cell	3.521	34.52	43502	0.11117	0.00095087
0.1 V	5.28	33.69	130	0.98081	0.00062103
0.4 V	5.167	34.08	21.87	4.288	0.00061285
0.8 V	5.051	34.77	43.41	3.403	0.00065349
1.2 V	5.271	33.15	42.99	2.085	0.00057278
1.6 V	5.229	34.03	142.5	1.71	0.00060615
2.0 V	5.257	34.07	121.2	1.286	0.00059131
2.4 V	4.696	36.63	1900	0.5963	0.0008227
2.8 V	5.404	33.59	6198	0.14753	0.0005505
3.0 V	5.434	32.41	1177	0.4356	0.0005667
potential (discharge)					
fresh cell	3.549	34.9	197.2	0.50259	0.00096776
0.005 V	5.316	33.61	52.09	2.905	0.00059505
0.1 V	4.944	35.44	31.64	13.15	0.00074467
0.4 V	5.154	34.44	1705	0.27517	0.00064492
0.8 V	5.305	33.49	8199	0.11801	0.00058928
1.6 V	5.357	32.17	1233	0.15983	0.00053856
2.0 V	5.361	32.74	167.5	1.31	0.00056654
2.4 V	5.328	32.23	153.6	1.224	0.00057353
2.8 V	5.2	32.07	578.8	0.84702	0.00064392

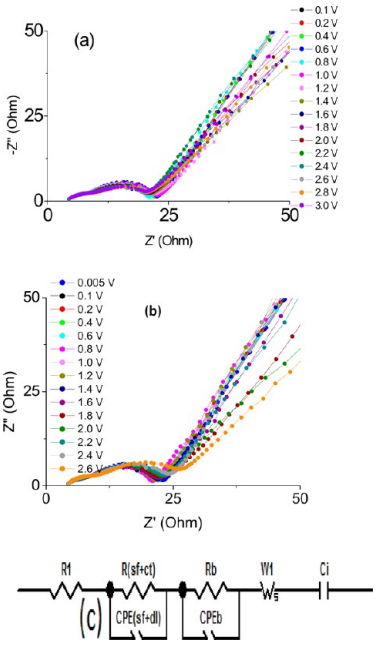

Figure 10. Nyquist plots ($-Z''$ vs. Z') of CoN (a) charge cycle , (b) discharge cycle, and (c) equivalent electrical circuit, voltage value are indicated in figures.

cycle onwards, no capacity fading took place and capacity was constant at 950 mAh g^{-1} till the last cycle (Table 1). The cell also displayed excellent coulombic efficiency.

The comparative first and second cycle discharge−charge cycling profiles of Co_3O_4, CoO, CoN are shown in Figure 6a,b. A slight variation in the discharge profiles are seen with during discharge and during charge cycle all compounds showed a plateaux at ∼2.0 V and it indicates role of crystal structure or morphology of Co_3O_4 or CoO or CoN will not influence or reduce the charge profile much. Morphology and crystal structure of three compounds play a role on the differences in the capacity values and minor impurity peaks (Figure 1a, c) will not play major role on electrochemical performance. In all cases, crystal structure destruction at end of 1st discharge−charge cycle and also long term cycling, this phenomena is well-documented in the above and other metal oxide anodes.[7] We note that for practical applications, further reduction of discharge−charge potentials is needed or advance research is needed. Additionally, further research my also be required for novel matching high-voltage cathode and electrolytes.

Cyclic Voltammetry Studies of Co_3O_4, CoO, and CoN. Cyclic voltammetry (CV) is used to complement galvanostatic cycling tests by analysing conversion reaction as well as redox potentials. CV was carried out at a scan rate of 58 $\mu V\ s^{-1}$. The voltage range used was 0.005 V to 3 V for 1 to 5 cycles. Lithium was used as the counter electrode. The cyclic voltammograms of all three compounds are shown in Figure 7. The main cathodic peak corresponds to reduction of Co-oxide or nitrides to metals and the main anodic peak corresponds to the reformation of corresponding oxides or nitride. The peaks observed in CV (Figure 7) closely resemble galvanostatic discharge−charge profiles (Figure 6). Broad peaks in the CV are due to structure destruction which leads to amorphization of the lattice. The main cathodic and anodic peaks potentials are close to previous reports.[7,27,30,36,37] The first cycle cathodic scan of CoO shows a continuous reduction in potential from the OCV of about 3.0 V to about 1.0 V. This is followed by a shoulder peak at 0.97 V. This is very similar to the first discharge−cycle profile during galvanostatic cycling. This is indicative of the partial reduction of CoO and also corresponds to the beginning of Li^+ ions insertion into the CoO crystal structure. Then there is a sharp voltage drop to 0.58 V. This is indicative of the destruction of the crystal structure and reduction of Co^{2+} to Co metal and the formation of Li_2O. The anodic scan showed a peak at 2.02 V. This shows the reformation of the CoO crystal structure. The second cathodic scan does not have the sharp voltage drop at 0.58 V. It instead occurs at 1.29 V and the drop is not as drastic. The anodic scan has a lower and more gentle peak at 2.10 V. This trend of decreasing potentials continues with the rest of the cycles as

dx.doi.org/10.1021/am4047552 | ACS Appl. Mater. Interfaces 2014, 6, 680−690

Table 4. Fitted impedance Values of CoN during Discharge and Charge Cycle at Selected Voltages

	R_1 (Ohm)	R(sf+ct) (Ohm)	R_b (Ohm)	CPE_b (F)	$CPE_{(sf+dl)}$ (F)
potential (charge)					
0.1 V	2.898	11.05	9.101	0.0001556	0.0019047
0.4 V	2.992	10.64	9.264	0.00015032	0.0016947
0.8 V	3.103	11.36	8.776	0.0001334	0.0017022
1.2 V	1.707	16.78	6.034	0.00011163	0.0040032
1.6 V	3.996	5.752	10.86	0.00027028	0.00013536
2.0 V	4.087	7.252	8.831	0.00019194	0.00014715
2.4 V	4.12	7.301	8.72	0.00024102	0.00012129
2.8 V	4.375	4.776	12.35	0.00055332	2.5392×10^{-5}
3.0 V	4.054	7.693	8.615	0.00028861	0.00018092
potential (discharge)					
0.005 V	3.16	11.62	8.715	0.000119	0.001736
0.1 V	2.946	2.95	9.293	0.00015608	0.0018317
0.4 V	3.067	10.19	9.25	0.00016062	0.001576
0.8 V	3.26	9.99	7.99	0.00012601	0.0014103
1.6 V	3.23	18.51	6.75	0.00015634	0.0055974
2.0 V	3.20	17.54	7.54	0.00011527	0.0043732
2.4 V	3.12	17.63	7.44	0.00010876	0.0045147
2.6 V	2.98	31.46	4.33	6.1015×10^{-5}	0.0050543

seen by the smaller peaks during both cathodic and anodic scans. The remaining 2-4 cycles overlap, showing good reversibility. However, the cell needs to be put through more cycles to conclusively say that the CoO cell shows good reversibility. The main cathodic and anodic peaks of CoN (Figure 7c) are close resemblance to CoO, during first cathodic scan doublets at 0.86 V and 0.65 V and a broad peak at 1.4 V vs. Li.

Electrochemical Impedance Spectroscopy (EIS) Studies on Co_3O_4, CoO, and CoN. Electrochemical impedance spectroscopy (EIS) is a one of the widely used and powerful analytical technique that is used to analyse electrode kinetics.[70−72,46,73] EIS was conducted after 60 galvanostatic discharge−charge cycles, impedance patterns were recorded over the frequency range of 0.35 MHz to 3mHz, with an Ac amplitude of 10 mV. The Nyquist plots ($-Z''$ vs. Z') were plotted and analyzed using Z-view software. Different equivalent circuit models are used for fitting experimental data based on best fit lines. We note that it is also possible to fit all experimental Nyquist plots using one single equivalent circuit, and we can expect a slight difference in the impedance values and they are within the experimental error. Equivalent circuit models gives information on the cell's complex behaviour to enable a better understanding of the cell's properties and extract impedance values. Our present proposed equivalent models are similar or slightly modified versions from the reported in previous papers.[72,74−76] This equivalent circuit is comprised of a R_1 (electrolyte resistance), R_{ct} (resistance during charge transfer), CPE_{dl} (double layer capacitance), R_{sf} (surface film resistance), CPE_{sf} (surface film capacitance), CPE_b (bulk capacitance), R_b (bulk resistance), W_1 (Warburg impedance), C_i (intercalation capacitance). Constant phase elements (CPE) represent the behavior of an imperfect capacitor due to the inhomogeneity of the electrode.

Co_3O_4. Nyquist (Z' vs. $-Z''$) plots are shown in Figure 8. The silent features of impedance studies are the semicircle flattens and becomes larger, indicating that resistance lowers. The semicircles seen at low frequency indicate bulk resistance.[72,73,77,78] Bulk resistance arises because of electronic conductivity of active material and ionic conductivity of electrolyte filled in pores of the composite electrode,[67,68] and high frequency region is surface film resistance which is arises due to due solid electrolyte interphase (SEI) and R_1 is the electrolyte resistance. The semicircle at medium frequency indicates charge transfer resistance which arises due to the electrode-electrolyte interface.[79,67,68,67,78,80] The fitted impedance values obtained using equivalent electrical circuit model at various discharge−charge voltages are given in Table 2. In general the impedance values are sensitive to the nature and crystal structure of the materials used. Overall total impedance values of Co_3O_4 cell were higher than CoO and CoN material. Present values are close to previous impedance studies by Kang et al.[81] and one other report on nanosized Co_3O_4[82] showed increase of charge transfer resistance values with cycle number, they correlated to decrease of capacity of capacity from 830 mAh g^{-1} after 2nd cycle to 200 mAh g^{-1} (after 60 cycles). It clearly shows that impedance values depend on the method of preparation of material, morphology, and electrode and cell fabrication technique.

CoO. The Nyquist plots of CoO cell during discharge and charge cycle are shown in Figure 9 and fitted impdance values are shown in Table 3. The overal impedance values are in the range 32-36 ohms at various volatages. Interestingly the overal total impedance values are low when compared the previous report on CoO prepared by using vapour phase reaction.[83] The probable reasons for variation of impedance values are due to difference cell design used to test the cell, morphology, and fabrication techniques. In the present case, lower resistance of CoO is due to good electrode kinetics when compared to Co_3O_4 and correlates well with galvanostatic cycling results.

CoN. The Nyquist plots of CoN are shown in Figure 10 and fitted impedance values are in range 5−11 Ohms during charge cycle (Table 4) and 2−31 Ohms during discharge cycles (Table 4). Impedance values of CoN clearly shows overall resistance of was lower when compared CoO and Co_3O_4. The observed decrease of impedance is correlated to differences in the crystal structure, ionic and electronic conductivity of the active material. Further careful studies are needed to evaluate this finding. Overall complementary impedance studies corroborates well with the observed trend in galvanostatic cycling.

CONCLUSIONS

Co_3O_4, CoO, and CoN were successfully prepared using bulk preparation methods. These materials were characterized using XRD, SEM, TEM and the Brunauer–Emmett–Teller (BET) surface methods. Galvanostatic cycling, cyclic voltammetry, and electrochemical impedance spectroscopy was performed to understand physical and chemical properties, analyse reaction mechanisms, electrode kinetics, capacity retention, and columbic efficiency. CoO and CoN showed the best performance. CoN was put through 60 cycles and capacity increased from the second cycle. The second cycle charge capacity was 875 mAh g^{-1} and the 60th charge cycle capacity was 956 mAh g^{-1}. The theoretical capacity is 1100 mAh g^{-1}. CoO displayed the most interesting results, with capacity increasing over the 60 cycles. The second charge cycle capacity was 790 mAh g^{-1} and the 60th charge cycle capacity was 893 mAh g^{-1}. The capacity had increased by 13%. Additionally, CoO had exceeded its theoretical capacity of 715 mAh g^{-1} from the very first charge cycle. An impedance spectroscopy study shows overall impedance is of the order of Co_3O_4>CoO>CoN. Cyclic voltammetry was performed on all three compounds to complement the galvanostatic cycling results and good reversibility of reactions was shown. Additionally, the main charge profiles for all three compounds are almost similar, even though the crystal structures differ and a slight difference in the electrochemical performance was noted with morphology. Overall, the bulk preparation methods had produced high-quality anode materials that far exceed the capacity. We note that for practical application further reduction of discharge–charge voltage are needed.

ASSOCIATED CONTENT

Supporting Information

Voltage vs. capacity and capacity vs. cycle number plots of Co_3O_4 at current rate of 120 mA g^{-1} .This material is available free of charge via the Internet at http://pubs.acs.org.

AUTHOR INFORMATION

Corresponding Author

*E-mail: phymvvr@nus.edu.sg, msemvvr@nus.edu.sg, or reddymvvr@gmail.com. Tel.:+65-65162607. Fax: +65-67776126.

Notes

The authors declare no competing financial interest.

ACKNOWLEDGMENTS

The authors thank the Gifted Education Branch of the Ministry of Education for granting the opportunity to take part in the Science Research Program (SRP) and also the Faculty of Science, NUS. G.P. thanks Mr .Yeo Jia Tian, St. Andrew's Junior College, for his assistance during the course of the SRP. M.V.R. thanks the National Research Foundation (NRF) Singapore NRF-CRP Grants R-144-000-295-281 and R-143-000-360-281. This project represented Singapore at the Intel International Science and Engineering Fair (ISEF) 2013 held in Phoenix, Arizona, USA. The authors also thank the American Chemical Society for awarding this project for the First Award at the ISEF 2013. This project also received the overall Second Award in the category of Chemistry in ISEF2013.

REFERENCES

(1) Baxter, J.; Bian, Z. X.; Chen, G.; Danielson, D.; Dresselhaus, M. S.; Fedorov, A. G.; Fisher, T. S.; Jones, C. W.; Maginn, E.; Kortshagen, U.; Manthiram, A.; Nozik, A.; Rolison, D. R.; Sands, T.; Shi, L.; Sholl, D.; Wu, Y. Y. *Energy Environ. Sci.* **2009**, *2*, 559–588.
(2) Goodenough, J. B.; Kim, Y. *Chem. Mater.* **2010**, *22*, 587–603.
(3) Wakihara, M. *Mater. Sci. Eng., R* **2001**, *33*, 109–134.
(4) Poizot, P.; Laruelle, S.; Grugeon, S.; Dupont, L.; Tarascon, J. M. *Nature* **2000**, *407*, 496–499.
(5) Das, B.; Reddy, M. V.; Malar, P.; Osipowicz, T.; Subba Rao, G. V.; Chowdari, B. V. R. *Solid State Ionics* **2009**, *180*, 1061–1068.
(6) Cabana, J.; Monconduit, L.; Larcher, D.; Palacin, M. R. *Adv. Mater.* **2010**, *22*, E170–E192.
(7) Reddy, M. V.; Subba Rao, G. V.; Chowdari, B. V. R. *Chem. Rev.* **2013**, *113*, 5364–5457.
(8) Cherian, C. T.; Reddy, M. V.; Haur, S. C.; Chowdari, B. V. R. *ACS Appl. Mater. Interfaces* **2013**, *5*, 918–923.
(9) Reddy, M. V.; Yu, C.; Jiahuan, F.; Loh, K. P.; Chowdari, B. V. R. *ACS Appl. Mater. Interfaces* **2013**, *5*, 4361–4366.
(10) Cherian, C. T.; Zheng, M.; Reddy, M. V.; Chowdari, B. V. R.; Sow, C. H. *ACS Appl. Mater. Interfaces* **2013**, *5*, 6054–6060.
(11) Xiao, Y.; Hao, D.; Chen, H. X.; Gong, Z. L.; Yang, Y. *ACS Appl. Mater. Interfaces* **2013**, *5*, 1681–1687.
(12) Li, Y. G.; Tan, B.; Wu, Y. Y. *Nano Lett.* **2008**, *8*, 265–270.
(13) Li, Y. G.; Wu, Y. Y. *Chem. Mater.* **2010**, *22*, 5537–5542.
(14) Le Viet, A.; Reddy, M. V.; Jose, R.; Chowdari, B. V. R.; Ramakrishna, S. *J. Phys. Chem. C* **2010**, *114*, 664–671.
(15) Zhu, P.; Wu, Y.; Reddy, M. V.; Nair, A. S.; Chowdari, B. V. R.; Ramakrishna, S. *RSC Advances* **2012**, *2*, 531–537.
(16) You, J. C.; Sheng, W. J.; Huang, K. K.; Hou, C. M.; Yue, H. J.; Hu, B.; Wang, M.; Wei, D. L.; Li, Q. W.; Zhao, L. P.; Dong, W. Y.; Zhao, Z. G.; Li, Y. J. *ACS Appl. Mater. Interfaces* **2013**, *5*, 2278–2282.
(17) Kim, J. G.; Shi, D. Q.; Kong, K. J.; Heo, Y. U.; Kim, J. H.; Jo, M. R.; Lee, Y. C.; Kang, Y. M.; Dou, S. X. *ACS Appl. Mater. Interfaces* **2013**, *5*, 691–696.
(18) Bhaskar, A.; Deepa, M.; Rao, T. N. *ACS Appl. Mater. Interfaces* **2013**, *5*, 2555–2566.
(19) Sen, U. K.; Mitra, S. *ACS Appl. Mater. Interfaces* **2013**, *5*, 1240–1247.
(20) Nethravathi, C.; Rajamathi, C. R.; Rajamathi, M.; Gautam, U. K.; Wang, X.; Golberg, D.; Bando, Y. *ACS Appl. Mater. Interfaces* **2013**, *5*, 2708–2714.
(21) Lang, L. M.; Xu, Z. *ACS Appl. Mater. Interfaces* **2013**, *5*, 1698–1703.
(22) Li, J. F.; Xiong, S. L.; Liu, Y. R.; Ju, Z. C.; Qian, Y. T. *ACS Appl. Mater. Interfaces* **2013**, *5*, 981–988.
(23) Huang, H.; Zhu, W. J.; Tao, X. Y.; Xia, Y.; Yu, Z. Y.; Fang, J. W.; Gan, Y. P.; Zhang, W. K. *ACS Appl. Mater. Interfaces* **2012**, *4*, 5974–5980.
(24) Binotto, G.; Larcher, D.; Prakash, A. S.; Urbina, R. H.; Hegde, M. S.; Tarascon, J. M. *Chem. Mater.* **2007**, *19*, 3032–3040.
(25) Nam, K. T.; Kim, D. W.; Yoo, P. J.; Chiang, C. Y.; Meethong, N.; Hammond, P. T.; Chiang, Y. M.; Belcher, A. M. *Science* **2006**, *312*, 885–888.
(26) Li, W. Y.; Xu, L. N.; Chen, J. *Adv. Funct. Mater.* **2005**, *15*, 851–857.
(27) Reddy, M. V.; Beichen, Z.; Nicholette, L. J.; Kaimeng, Z.; Chowdari, B. V. R. *Electrochem. Solid-State Lett.* **2011**, *14*, A79–A82.
(28) Reddy, M. V.; Beichen, Z.; Loh, K. P.; Chowdari, B. V. R. *CrystEngComm* **2013**, *15*, 3568–3574.
(29) Yang, R. Z.; Wang, Z. X.; Liu, J. Y.; Chen, L. Q. *Electrochem. Solid-State Lett.* **2004**, *7*, A496–A499.
(30) Varghese, B.; Hoong, T. C.; Yanwu, Z.; Reddy, M. V.; Chowdari, B. V. R.; Wee, A. T. S.; Vincent, T. B. C.; Lim, C. T.; Sow, C. H. *Adv. Funct. Mater.* **2007**, *17*, 1932–1939.
(31) Sun, Y.; Hu, X.; Luo, W.; Huang, Y. *J. Mater. Chem.* **2012**, *22*, 13826–13831.
(32) Guan, H.; Wang, X.; Li, H.; Zhi, C.; Zhai, T.; Bando, Y.; Golberg, D. *Chem. Commun.* **2012**, *48*, 4878–4880.

(33) Sun, Y. M.; Hu, X. L.; Luo, W.; Huang, Y. H. *J. Phys. Chem. C* **2012**, *116*, 20794−20799.
(34) Zhang, H. J.; Tao, H. H.; Jiang, Y.; Jiao, Z.; Wu, M. H.; Zhao, B. *J. Power Sources* **2010**, *195*, 2950−2955.
(35) Ryu, W. H.; Shin, J.; Jung, J. W.; Kim, I. D. *Journal of Materials Chemistry A* **2013**, *1*, 3239−3243.
(36) Das, B.; Reddy, M. V.; Subba Rao, G. V.; Chowdari, B. V. R. *J. Mater. Chem.* **2012**, *22*, 17505−17510.
(37) Das, B.; Reddy, M. V.; Chowdari, B. V. R. *Nanoscale* **2013**, *5*, 1961−1966.
(38) Liu, T. C.; Pell, W. G.; Conway, B. E.; Roberson, S. L. *J. Electrochem. Soc.* **1998**, *145*, 1882−1888.
(39) Choi, D.; Blomgren, G. E.; Kumta, P. N. *Adv. Mater.* **2006**, *18*, 1178−1182.
(40) Lekitima, J. N.; Ozoemena, K. I.; Jafta, C. J.; Kobayashi, N.; Song, Y.; Tong, D.; Chen, S.; Oyama, M. *J. Mater. Chem. A* **2013**, *1*, 2821−2826.
(41) Hulicova, D.; Kodama, M.; Hatori, H. *Chem. Mater.* **2006**, *18*, 2318−2326.
(42) Kartachova, O.; Glushenkov, A. M.; Chen, Y. H.; Zhang, H. Z.; Chen, Y. *J. Mater. Chem. A* **2013**, *1*, 7889−7895.
(43) Das, B.; Reddy, M. V.; Subba Rao, G. V.; Chowdari, B. V. R. *J. Solid State Electrochem.* **2008**, *12*, 953−959.
(44) Das, B.; Reddy, M. V.; Krishnamoorthi, C.; Tripathy, S.; Mahendiran, R.; Subba Rao, G. V.; Chowdari, B. V. R. *Electrochim. Acta* **2009**, *54*, 3360−3373.
(45) Reddy, M. V.; Subba Rao, G. V.; Chowdari, B. V. R. *J. Power Sources* **2010**, *195*, 5768−5774.
(46) Reddy, M. V.; Sakunthala, A.; SelvashekaraPandian, S.; Chowdari, B. V. R. *J. Phys. Chem. C* **2013**, *117*, 9056−9064.
(47) Reddy, M. V.; Kenrick, K. Y. H.; Wei, T. Y.; Chong, G. Y.; Leong, G. H.; Chowdari, B. V. R. *J. Electrochem. Soc.* **2011**, *158*, A1423−A1430.
(48) Prabu, M.; Reddy, M. V.; Selvasekarapandian, S.; Subba Rao, G. V.; Chowdari, B. V. R. *Electrochim. Acta* **2012**, *85*, 572−578.
(49) Godillot, G.; Guerlou-Demourgues, L.; Croguennec, L.; Shaju, K. M.; Delmas, C. *J. Phys. Chem. C* **2013**, *117*, 9065−9075.
(50) Reddy, M. V.; Yu, C.; Jiahuan, F.; Loh, K. P.; Chowdari, B. V. R. *RSC Advances* **2012**, *2*, 9619−9625.
(51) Wang, X.; Guan, H.; Chen, S. M.; Li, H. Q.; Zhai, T. Y.; Tang, D. M.; Bando, Y.; Golberg, D. *Chem. Commun.* **2011**, *47*, 12280−12282.
(52) Wang, X.; Wu, X. L.; Guo, Y. G.; Zhong, Y. T.; Cao, X. Q.; Ma, Y.; Yao, J. N. *Adv. Funct. Mater.* **2010**, *20*, 1680−1686.
(53) Bian, S. W.; Zhu, L. *RSC Advances* **2013**, *3*, 4212−4215.
(54) Feng, X. Y.; Shen, C.; Yu, Y.; Wei, S. Q.; Chen, C. H. *J. Power Sources* **2013**, *230*, 59−65.
(55) Kim, G. P.; Park, S.; Nam, I.; Park, J.; Yi, J. *Journal of Materials Chemistry A* **2013**, *1*, 3872−3876.
(56) Kyerematen, N. A.; Lebouin, C.; Knauth, P.; Djenizian, T. *Electrochim. Acta* **2013**, *88*, 814−820.
(57) Li, D.; Shi, D. Q.; Chen, Z. X.; Liu, H. K.; Jia, D. Z.; Guo, Z. P. *RSC Advances* **2013**, *3*, 5003−5008.
(58) Li, X. F.; Wang, C. L. *J. Mater. Chem. A* **2013**, *1*, 165−182.
(59) Rui, X. H.; Tan, H. T.; Sim, D. H.; Liu, W. L.; Xu, C.; Hng, H. H.; Yazami, R.; Lim, T. M.; Yan, Q. Y. *J. Power Sources* **2013**, *222*, 97−102.
(60) Sun, H. Y.; Ahmad, M.; Zhu, J. *Electrochim. Acta* **2013**, *89*, 199−205.
(61) Yang, X. L.; Fan, K. C.; Zhu, Y. H.; Shen, J. H.; Jiang, X.; Zhao, P.; Luan, S. R.; Li, C. Z. *ACS Appl. Mater. Interfaces* **2013**, *5*, 997−1002.
(62) Zhuo, L. H.; Wu, Y. Q.; Ming, J.; Wang, L. Y.; Yu, Y. C.; Zhang, X. B.; Zhao, F. Y. *J. Mater. Chem. A* **2013**, *1*, 1141−1147.
(63) Liu, D. Q.; Wang, X.; Wang, X. B.; Tian, W.; Bando, Y.; Golberg, D. *Sci. Rep.* **2013**, *3*.
(64) Wu, F. D.; Wang, Y. *J. Mater. Chem.* **2011**, *21*, 6636−6641.
(65) Sun, Y. M.; Hu, X. L.; Luo, W.; Huang, Y. H. *J. Mater. Chem.* **2012**, *22*, 13826−13831.
(66) Cherian, C. T.; Sundaramurthy, J.; Reddy, M. V.; Suresh Kumar, P.; Mani, K.; Pliszka, D.; Sow, C. H.; Ramakrishna, S.; Chowdari, B. V. R. *ACS Appl. Mater. Interfaces* **2013**, *5*, 9957−9963.
(67) Wu, Y.; Reddy, M. V.; Chowdari, B. V. R.; Ramakrishna, S. *ACS Appl. Mater. Interfaces* **2013**, *5*, 12175−12184.
(68) Varghese, B.; Reddy, M. V.; Yanwu, Z.; Lit, C. S.; Hoong, T. C.; Subba Rao, G. V.; Chowdari, B. V. R.; Wee, A. T. S.; Lim, C. T.; Sow, C. H. *Chem. Mater.* **2008**, *20*, 3360−3367.
(69) Reddy, M. V.; Pecquenard, B.; Vinatier, P.; Levasseur, A. *Electrochem. Commun.* **2007**, *9*, 409−415.
(70) Levi, M. D.; Aurbach, D. *J. Phys. Chem. B* **1997**, *101*, 4630−4640.
(71) Croce, F.; Nobili, F.; Deptula, A.; Lada, W.; Tossici, R.; D'Epifanio, A.; Scrosati, B.; Marassi, R. *Electrochem. Commun.* **1999**, *1*, 605−608.
(72) Reddy, M. V.; Madhavi, S.; Subba Rao, G. V.; Chowdari, B. V. R. *J. Power Sources* **2006**, *162*, 1312−1321.
(73) Sakunthala, A.; Reddy, M. V.; Selvasekarapandian, S.; Chowdari, B. V. R.; Selvin, P. C. *J. Phys. Chem. C* **2010**, *114*, 8099−8107.
(74) Nobili, F.; Dsoke, S.; Croce, F.; Marassi, R. *Electrochim. Acta* **2005**, *50*, 2307−2313.
(75) Reddy, M. V.; Subba Rao, G. V.; Chowdari, B. V. R. *J. Mater. Chem.* **2011**, *21*, 10003−10011.
(76) Reddy, M. V.; Wei Wen, B. L.; Loh, K. P.; Chowdari, B. V. R. *ACS Appl. Mater. Interfaces* **2013**, *5*, 7777−7785.
(77) Reddy, M. V.; Subba Rao, G. V.; Chowdari, B. V. R. *J. Phys. Chem. C* **2007**, *111*, 11712−11720.
(78) Zaban, A.; Zinigrad, E.; Aurbach, D. *J. Phys. Chem.* **1996**, *100*, 3089−3101.
(79) Aurbach, D.; Zaban, A. *J. Electrochem. Soc.* **1994**, *141*, 1808−1819.
(80) Reddy, M. V.; Jose, R.; Le Viet, A.; Ozoemena, K. I.; Chowdari, B. V. R.; Ramakrishna, S., *Electrochim. Acta.* 2013 (in press, DOI: 10.1016/j.electacta.2013.10.003).
(81) Kang, Y.-M.; Song, M.-S.; Kim, J.-H.; Kim, H.-S.; Park, M.-S.; Lee, J.-Y.; Liu, H. K.; Dou, S. X. *Electrochim. Acta* **2005**, *50*, 3667−3673.
(82) Kang, J. G.; Ko, Y. D.; Park, J. G.; Kim, D. W. *Nanoscale Res. Lett.* **2008**, *3*, 390−394.
(83) Barreca, D.; Cruz-Yusta, M.; Gasparotto, A.; Maccato, C.; Morales, J.; Pozza, A.; Sada, C.; Sánchez, L.; Tondello, E. *J. Phys. Chem. C* **2010**, *114*, 10054−10060.